Dynamic state of low-Reynolds-number turbulent channel flow

Hiroya Mamori[*]

Department of Mechanical and Intelligent Systems Engineering, The University of Electro-Communications,
1-5-1, Chofugaoka, Chofu, Tokyo 182-8585, Japan

Yusuke Nabae, Shingo Fukuda, and Hiroshi Gotoda[†]

Department of Mechanical Engineering, Tokyo University of Science, 6-3-1 Niijuku, Katsushika-ku, Tokyo 125-8585, Japan

We numerically study the dynamic state of a low-Reynolds-number turbulent channel flow from the viewpoints of symbolic dynamics and nonlinear forecasting. A low-dimensionally (high-dimensionally) chaotic state of the streamwise velocity fluctuations emerges at a viscous sublayer (logarithmic layer). The possible presence of the chaotic states is clearly identified by orbital instability-based nonlinear forecasting and ordinal partition transition network entropy in combination with the surrogate data method.

I. INTRODUCTION

Since the outstanding discovery of Lorenz chaos [1] representing the atmospheric turbulent flow, nonlinear time series analysis based on dynamical systems theory has steadily been developed over the last 20 years and has become a valuable tool for revealing the complex dynamics appearing in several different scientific disciplines, with possible applications in biology, medicine, electrical, and mechanical engineering [2–4]. It has undoubtedly constituted a firm platform for extracting the deterministic chaos in randomly fluctuating physical quantities, focusing mainly on two important features: (i) fractal as a self-similarity structure and (ii) short-range forecastability and long-range unforecastability associated with strong sensitivity to initial conditions in dynamical systems. Orbital-instability-based forecasting [5] ensures a reasonable performance in the short-range prediction of chaotic dynamics [2]. This method can be considered an inverse approach in the sense that underlying dynamics is expressed by a forecasting model constructed from the observed temporal behavior. Gotoda and coworkers have shown that the orbital-instability-based forecasting method (OIFM), incorporating the updated library data in phase space, which is an extended version of the Sugihara-May algorithm [5], is valid for extracting the short-range predictability and long-range unpredictability features of chaotic dynamics in various complex nonlinear phenomena [6–9].

Recent substantial breakthroughs in ordinal-pattern-based analysis, in terms of symbolic dynamics [10], have recently opened a way to explore the deterministic nature of complex spatiotemporal dynamics. The most fundamental quantity obtained by ordinal-pattern-based analysis is permutation entropy [11], considering the probability distribution of ordinal patterns in a time series. Permutation entropy enables us to

quantify the randomness of aperiodic fluctuations in a wide spectrum of fluid systems [7,12–15]. On the basis of the Bandt-Pompe concept [11], an ordinal-pattern-based complex network in accordance with the Markov chain, namely, the ordinal partition transition network (OPTN), has been proposed by Small and coworkers [16,17]. The network consists of nodes (ordinal patterns) and links between nodes (transition probability between ordinal patterns). Gotoda and coworkers [8,9,18,19] have more recently shown the applicability of OPTN entropy for examining complex dynamic behaviors in various chemically reacting fluids.

Wall turbulence, which is the most well-recognized class of shear turbulent flow, possesses strong aperiodic velocity fluctuations in both space and time, in accordance with Kolmogorov's five-third scaling law in power spectra. Direct numerical simulation (DNS) of wall turbulence has led to the identification of a rich variety of prominent coherent structures involving high-low-speed streaks and hairpin vortices [20]. The discovery of these coherent structures implies that it is inadequate to describe aperiodic fluctuations in a wall-turbulent flow as entirely random events. The identification of a deterministically chaotic state in seemingly randomlike fluid motions is a challenging and longstanding topic in contemporary fluid physics and various disciplines of nonlinear science. Thus far, many previous studies [21–26] using DNS have revealed the details of coherent structures in a wall-turbulent flow in a broad range of Reynolds numbers. However, notwithstanding the progress in DNS over a long period of wall-turbulent flow research, the dynamic state and short-range forecastability of the flow velocity field still remain unexplored, even for a low-Reynolds-number turbulent channel flow, from the viewpoints of symbolic dynamics and nonlinear forecasting.

Our main aim in this paper is to clarify the dynamic state and short-range forecastability of streamwise velocity in a low-Reynolds-number turbulent channel flow, focusing on two sophisticated analytical methods: OIFM and OPTN. Recent advances in machine-learning technology have led

---

[*]Corresponding author: mamori@uec.ac.jp

[†]gotoda@rs.tus.ac.jp

to deserve time series prediction methods such as long short-term memory networks [27] and reservoir computing (RC) [28,29]. These supervised machine-learning methods belong to a subclass of recurrent neural networks. The applicability of RC as the model-free prediction of chaos has been highlighted in many numerical studies on various fluid dynamics and related nonlinear dynamical systems [30–41]. In this paper, we compare the forecastability of streamwise velocity obtained by OIFM and that obtained by RC.

II. NUMERICAL COMPUTATION AND ANALYTICAL METHODS

We perform the DNS of a fully developed and incompressible turbulent channel flow under a constant pressure gradient condition. We solve the same governing equations, that is, the continuity and Navier-Stokes equations, as those in a previous study [42]. The no-slip boundary conditions are imposed on the flow velocities on walls, and the periodic boundary conditions are applied in the streamwise and spanwise directions. All the simulations start from the fully developed and turbulent velocity field. The DNS code is based on Ref. [42] for the spatial discretization, energy-conservative second-order finite difference method; for the time integration, the low-storage third-order Runge–Kutta/Crank–Nicolson method; and for the velocity-pressure coupling, a higher-order SMAC-like method. A fast Fourier transform and a tridiagonal matrix solver are used for the pressure Poisson equation in the homogeneous and wall-normal directions, respectively. The friction Reynolds number $Re_\tau (= u_\tau^* \delta^*/\nu^*$, where ν^* is the kinematic viscosity, δ^* is the channel half-width, and u_τ^* is the friction velocity) is set to be 180 as a representative low-Reynolds-number turbulent flow, and corresponds to the bulk Reynolds number $Re_b (= 2u_b^* \delta^*/\nu^*$, where u_b^* is the bulk mean velocity.) ≈ 5600. We set the computational domain $(= L_x \times L_y \times L_z)$, number of grid points $(= N_x \times N_y \times N_z)$, and the time resolution Δt^+ to $4\pi \times 2 \times \pi$, $256 \times 96 \times 128$, and 9×10^{-2}, respectively. We confirm that the profiles of statistics, that is, the mean velocity profile and the root-mean square of the velocity fluctuations, are in good agreement with the DNS database obtained by Moser *et al.* [22]. Note that the viscous sublayer corresponds to $y^+ < 6$, the buffer layer corresponds to $6 \lesssim y^+ \lesssim 30$, and the logarithmic layer corresponds to $y^+ > 30$.

We estimate the OPTN entropy [17,18] of streamwise velocity

$$S_t = -\sum_{i=1}^{D_e!^2} \sum_{j=1}^{D_e!^2} w_{ij} \ln w_{ij} / \ln D_e!^2$$

in this paper. The components of the adjacency matrix w_{ij} correspond to the transition probability from a permutation pattern of streamwise velocity $\pi_i (i = 1, 2, ..., D_e!)$ to $\pi_j (j = 1, 2, ..., D_e!)$. Nomi *et al.* [9] have recently proposed a method to determine a suitable value of D_e, focusing on the possible presence of transition patterns in the OPTN. Missing permutation (ordinal) patterns [43] of a time series appear for deterministic dynamics, whereas they do not appear for stochastic dynamics [44]. They have reported that missing transition patterns appear at $D_e \geqslant 4$ for Gaussian noise and

Brownian motion [9], which means that D_e should be set to 3 for the construction of the OPTN. On this basis, we set D_e to 3 for the estimation of S_t. If the temporal evolution of the streamwise velocity u is monotonically increasing or decreasing, S_t takes zero, observing only one transition permutation pattern. If the temporal evolution of u is governed by a completely random process, S_t takes unity owing to the formation of a uniform transition probability distribution for ordinal patterns. In this paper, we use the surrogate data method [45] for u, which is a popular statistical test for validating nonlinear determinism in an irregular time series. The null hypothesis of surrogate data we considered in this paper is that a Gaussian linear random process governs the irregular components of a time series, preserving the probability density function and power spectra of the original time-series data.

For the OIFM [7], u is first divided into two parts: the library data and reference data set. After constructing the D_e-dimensional phase space consisting of $\mathbf{u} = (u(t_i^+), u(t_i^+ + \tau_e^+), ..., u(t_i^+ + \tau_e^+(D_e - 1)))$ from the library data, we obtain the predicted point $\hat{\mathbf{u}}(t_f^+ + T^+)$ of a trajectory in the phase space

$$\hat{\mathbf{u}}(t_f^+ + T^+) = \frac{\sum_{k=1}^K \mathbf{u}(t_k^+ + T^+)\exp(-\|\mathbf{u}(t_f^+) - \mathbf{u}(t_k^+)\|)}{\sum_{k=1}^K \exp(-\|\mathbf{u}(t_f^+) - \mathbf{u}(t_k^+)\|)},$$

where $\mathbf{u}(t_k^+)$ is a point near the final point $\mathbf{u}(t_f^+)$ of the trajectory in the phase space. Here, τ_e^+ is the delay time in the phase space, T^+ is the time step, and K is the number of nearby points. The temporal evolution of the predicted $\hat{u}(t_f^+ + T^+)$ is inversely obtained from $\hat{\mathbf{u}}(t_f^+ + T^+)$. An important point in this method is the update of the library data to continue the capturing of determinism in the current temporal dynamics, maintaining the size of the library data constant. We systematically change the duration t_p^+ of the actual temporal evolution of u added to the library data, where t_p^+ corresponds to predictable time. We examine the short-range predictability feature by estimating the correlation coefficient C between the predicted $\hat{u}(t_f^+ + T^+)$ and the reference $u(t_f^+ + T^+)$ as a function of t_p^+. In accordance with a numerical study [44] on missing patterns of a time series and the false nearest neighboring method [46], D_e is set to 5 for the OIFM. Note that the suitable value of D_e is not identical to that for the OPTN on the basis of a type of ordinal pattern which one has to consider. In a preliminary test, we systematically varied K from 20 to 100. The values of K within this range were found to have little effect on C. We set K to 50 in this study. Both τ_e^+ and T^+ are set to 1.08 so as to sufficiently capture visible determinism in terms of the statistical complexity [47] and orbital instability in phase space. Note that u at $0 \leqslant t^+ \leqslant 5000$ are used for the library data, whereas those at $5000 < t^+ \leqslant 9000$ are used as reference data for the predicated u.

For RC, we first construct an input layer, a reservoir network, and a linear output layer. The update equation of the state vector $\mathbf{r}$ of the reservoir network is defined as

$$\mathbf{r}(t_i^+ + T^+) = (1 - \alpha)\mathbf{r}(t_i^+) + \alpha \tanh[\mathbf{W}\mathbf{r}(t_i^+) + \mathbf{W}_{\text{in}}\mathbf{u}(t_i^+)],$$

where $\mathbf{u}$ is the input vector of streamwise velocity and α is the leakage rate. Here, $0 < \alpha \leqslant 1$. We use u at $0 \leqslant t^+ \leqslant 5000$ for training the reservoir computer. The matrices $\mathbf{W}$ and $\mathbf{W}_{\text{in}}$

represent the weight of the internal connection of reservoir nodes and the weight of the input, respectively. $\mathbf{W}$ consists of the $D_r \times D_r$ adjacency matrix and includes a sparse random matrix with nonzero components. Similar to a recent study [36], $D_r = 1500$ and the number of nonzero components is set to 20% of the total number of the adjacency matrix elements ($= 450\,000$). The elements in the matrix $\mathbf{W}$ have a uniform distribution. The output vector $\mathbf{v}$ of the reservoir system is taken to be a linear function of the reservoir state and the input vector.

$$\mathbf{v}(t_i^+) = \mathbf{W}_{\text{out}} \begin{pmatrix} 1 \\ \mathbf{u}(t_i^+) \\ \mathbf{r}(t_i^+) \end{pmatrix},$$

where $\mathbf{W}_{\text{out}}$ is the solely adjusted matrix in the training stage. On the basis of Tikhonov-Arsenin regularization [48], we optimize $\mathbf{W}_{\text{out}}$ by minimizing the error between the output data $\mathbf{v}$ and the training data $\mathbf{v}_d$ (see Ref. [36] on the mathematical formula of $\mathbf{W}_{\text{out}}$ and the setting value of the regularization coefficient). Here, $\mathbf{u}(t_i^+) = (1; u(t_i^+))$ and $\mathbf{v}_d(t_i^+) = u(t_i^+ + T^+)$. We use $\mathbf{u}(t_i^+) = (1; u_o(t_i^+))$ every t_p^+ in the forecasting process and finally obtain the output vector $\mathbf{v}(t_i^+) = u_p(t_i^+ + T^+)$, where the subscript $o(p)$ denotes the original (predicted) data. This forecasting process is adopted for $5000 < t^+ \leqslant 9000$.

III. RESULTS AND DISCUSSION

Figure 1 shows the temporal evolution of the streamwise velocity u at $y^+ = 4$ and 35, together with the instantaneous flow velocity field on the x-z plane. u exhibits aperiodic fluctuations in the viscous sublayer during a wall-turbulent flow. This is strongly associated with the formation of low-high-speed streaks. The structural destabilization of these streaks and the subsequent formation (collapse) of streamwise vortices via a three-dimensional nonlinear process give rise to coherent structures with various scales and strengths in the buffer layer. The irregularity and amplitude of u notably increase in the logarithmic layer owing to the complex spatiotemporal dynamics of the coherent structures. The encompassing physical mechanism by which these complex behaviors emerge is mainly explained by the self-sustaining process of wall turbulence [20].

Figure 2 shows the frequency distributions of the OPTN entropy S_t for the original and surrogate data at $y^+ = 4$ and 35. In this paper, the number of surrogate data sets is 10 000. S_t for the original data is approximately 0.53 (0.81) at $y^+ = 4$ ($y^+ = 35$). The value of S_t for the original data at $y^+ = 4$ does not correspond to those for all the surrogate data sets, which clearly shows the rejection of the hypothesis. In contrast, the value of S_t for the original data at $y^+ = 35$ coincides with those of 6 from 10 000 surrogate data sets. However, the hypothesis can be sufficiently rejected with 99.9% reliability as determined by a t test of estimates of S_t for the surrogate data sets. This indicates the possible presence of a nonlinear deterministic process at both the viscous sublayer and logarithmic layer.

Figure 3 shows the temporal evolutions of the original and predicted u at $y^+ = 4$, together with the power spectrum and
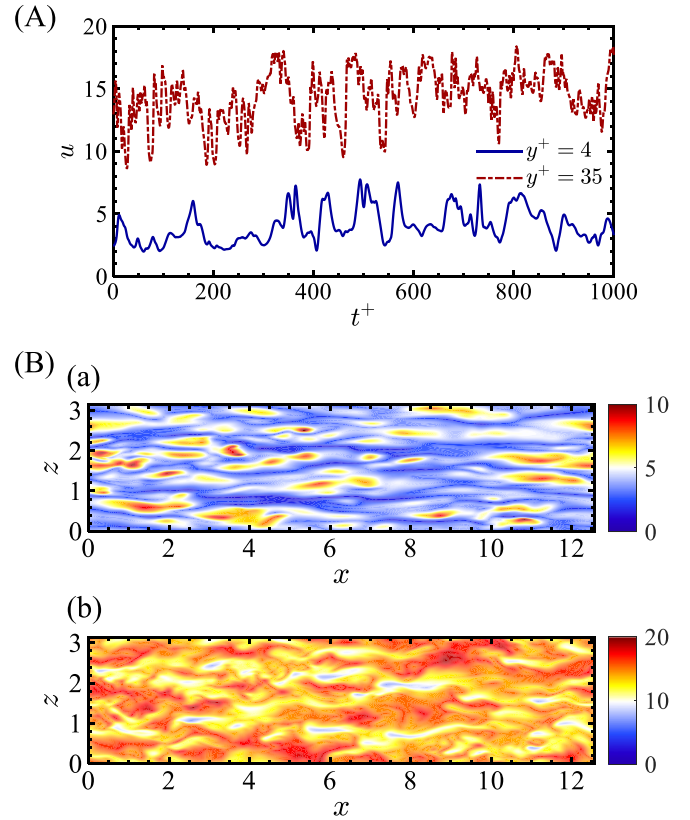

FIG. 1. (A) Temporal evolution of streamwise velocity u. (B) Instantaneous streamwise velocity field u on x-z plane. (a) $y^+ = 4$ and (b) $y^+ = 35$.

probability density distribution. Here, $\tau^+ = 1.08$. Note that the original (predicted) u denotes u_o (u_p). u_p at $y^+ = 4$ nearly coincides with that of u_o. The power density of u_o in terms of f^+ exhibits a scaling-law decay with the exponent $-5/3$; this is an important feature of a well-developed turbulent flow. The power density distribution of u_p coincides with that of u_o in a wide range of frequencies. The probability density distribution of u_p is also in good agreement with that of u_o. Note that we observe a similar coincidence of the power spectrum and probability density distribution for u_p at $y^+ = 35$.
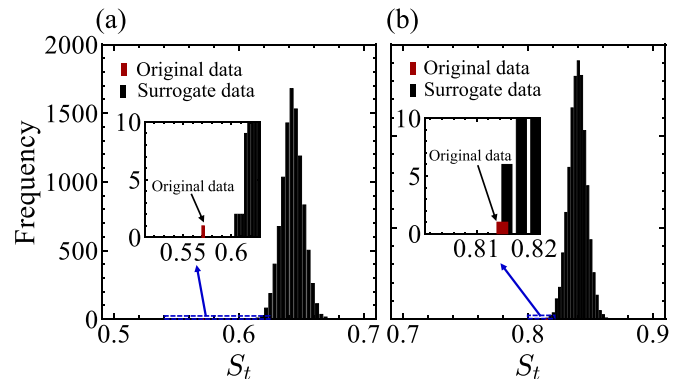

FIG. 2. Frequency distributions of the OPTN entropy S_t for the original and surrogate data. (a) $y^+ = 4$ and (b) $y^+ = 35$. Here, the sampling interval $\tau^+ = 1.08$.
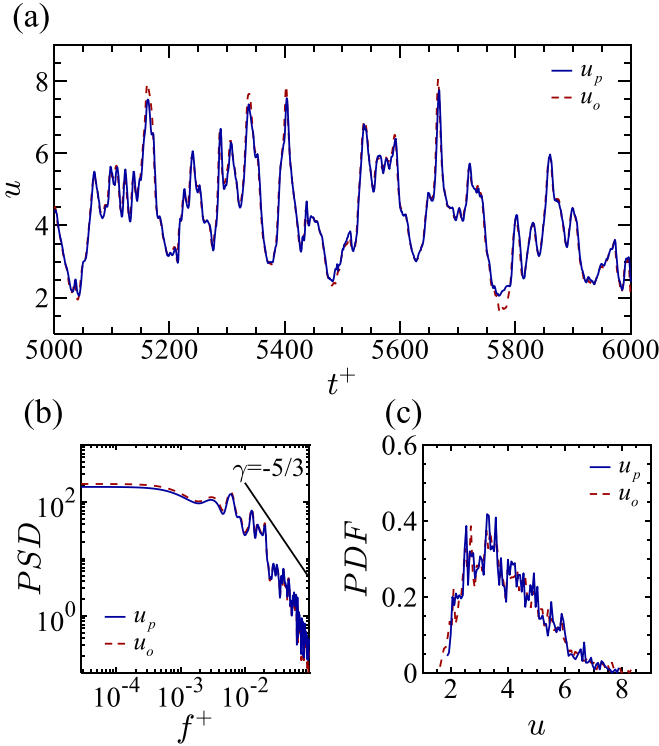
FIG. 3. (a) Temporal evolutions of the original streamwise velocity u_o and predicted streamwise velocity u_p at $y^+ = 4$, together with (b) power spectrum and (c) probability density distribution. Here, the sampling interval $\tau^+ = 1.08$.

These findings show that the OIFM can reproduce the power spectrum and probability density distribution of streamwise velocity in both the viscous sublayer and logarithmic layer.

Figure 4(a) shows the variation in the correlation coefficient C between u_o and u_p at $y^+ = 4$ and 35 as a function of the predicable time t_p^+. Here, τ^+ is set to 1.08. For $y^+ = 4$, C at $t_p^+ = 1.08$ is approximately 0.99 with high predictive accuracy. It decreases exponentially with increasing t_p^+, indicating the regime of short-range forecastability and long-range unforecastability. This is a typical feature of chaos based on orbital instability in phase space. A similar trend
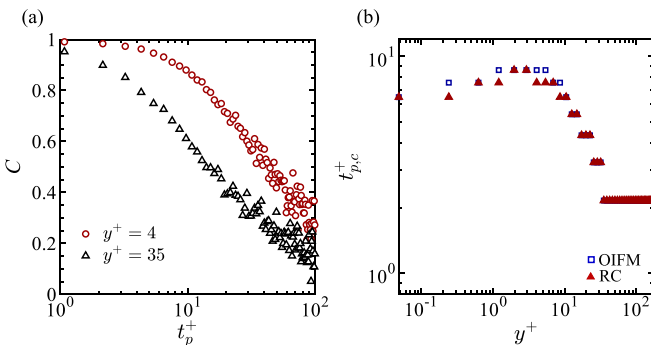

FIG. 4. (a) Variation in the correlation coefficient C between u_o and u_p at $y^+ = 4$ and 35 as a function of the predicable time t_p^+ for the OIFM. (b) Variation in the predicable time $t_{p,c}^+$ in terms of y^+ for the OIFM and RC. Here, the sampling interval $\tau^+ = 1.08$.

is obtained for $y^+ = 35$, showing a slight decrease in predictive accuracy in the entire range of t_p^+. The results shown in Figs. 2–4(a) demonstrate that the dynamic state of streamwise velocity represents the low- and high-dimensional chaotic states at the viscous sublayer and logarithmic layer, respectively. Low-dimensional chaos can be produced by numerically solving high-dimensional dynamical systems with infinity freedom such as the Navier–Stokes equation. However, no numerical or theoretical studies have extracted low-dimensional chaos in a well-developed wall-turbulent flow. The advanced methodologies based on nonlinear forecasting and complex networks we employed in this paper enables us to find hidden low-dimensional chaos in a well-developed wall-turbulent flow. The variation in the predictable time $t_{p,c}^+$ in terms of y^+ for the OIFM and RC is shown in Fig. 4(b). Here, $t_{p,c}^+$ is defined as t_p^+ at which C is 0.9. $t_{p,c}^+$ for the OIFM is approximately 8.6 at $1 < y^+ \lesssim 5$ and monotonically decreases to 2.2 at y^+ higher than 35 near the boundary between the buffer and logarithmic layers. It remains nearly unchanged at $y^+ \gtrsim 31$ at the logarithmic layer. The most interesting and important point to emphasize here is that the predicable time at $y^+ = 4(y^+ = 35)$ is approximately 100 (20) times the time resolution of DNS. This means that the OIFM has potential for use in predicting the streamwise velocity in a wide variety of layers such as the viscous sublayer, buffer, and logarithmic layers in a low-Reynolds-number channel flow. In contrast, $t_{p,c}^+$ for RC is shorter than that for the OIFM at $y^+ \lesssim 10$ and corresponds to that for the OIFM in the logarithmic layers. An important point to note here is the decrease in the predictability of u in the viscous sublayer and buffer layer. Many numerical studies have reported that RC is well-suited for the prediction of low-dimensional and high-dimensional chaos. In particular, Chen *et al.* [35] have shown that for the Lorenz chaos, the geometric metrics including the correlation dimension and the multiscale entropy are nearly identical between the original reference data and the predicted data. In this sense, RC ensures sufficient prediction performance of low-dimensional chaos. We do not adopt any potential recurrent neural networks in this paper, but at least RC does not necessarily yield a superior prediction of low-dimensional chaotic streamwise velocity fluctuations in a wall-turbulent flow. This enables us to reaffirm the significance of the temporal evolution of orbits in the phase space on the basis of the embedding theorem [49].

Figure 5 shows the variation in C between u_o and u_p as a function of the sampling interval τ^+ for different y^+ locations. C decreases with τ^+ at all y^+ locations, which indicates that the coarse graining of u reduces the predictability of u. C takes high values at $4 \leqslant y^+ \lesssim 8$, with high short-term forecastability of streamwise velocity in the viscous sublayer. The high short-term forecastable region can be arranged by u_τ and corresponds to the scaling region in the root-mean square of u. The profile of the root-mean square does not nearly change at $y^+ \lesssim 8$ regardless of the friction Reynolds number [22,26]. This provides us an important physical interpretation that the high short-term forecastability of the streamwise velocity explains the emergence of the universal streak structure without the dependency on the Reynolds numbers. The variations in S_t for u_o and u_p are shown in Fig. 6 as a function of τ^+ at
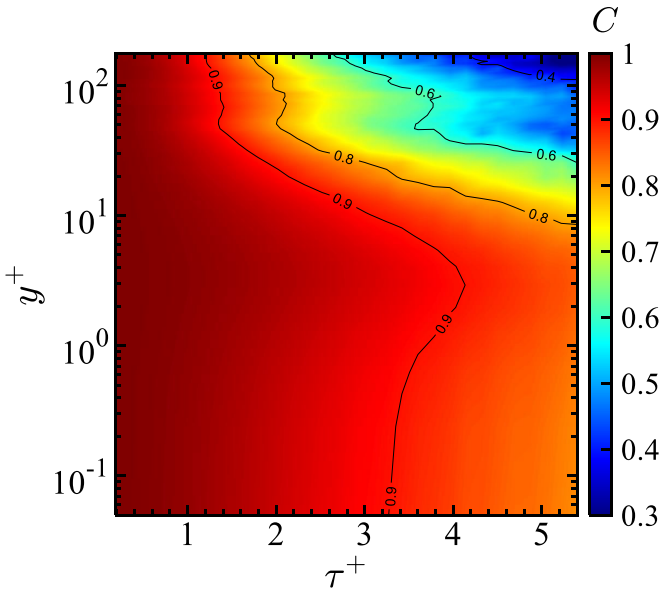
FIG. 5. Variation in the correlation coefficient C between u_o and u_p as a function of the sampling interval τ^+ at different y^+.

FIG. 6. Variation in the OPTN entropy S_t for (a) u_o and (b) u_p as a function of the sampling interval τ^+ at different vertical y^+ locations.

different y^+ locations. S_t for the original data increases with τ^+ at all y^+ locations. On the basis of the results shown in Fig. 5, the decrease in the predictability of u in terms of τ^+ is strongly associated with the high randomness due to the coarse graining of u. S_t significantly decreases at $4 \lesssim y^+ \lesssim 8$, indicating that the dynamic behavior of streamwise velocity possesses a high determinism in the viscous sublayer. An important finding in Fig. 6 is that the distribution of S_t for u_p shows a fair correspondence to that for u_o. This clearly shows that u_p preserves the randomness of u_o. Thus far, the root-mean square, power spectrum, and probability density function have been used to evaluate the predictive performance of wall-turbulent flows. The results shown in Fig. 6 also indicate that OPTN entropy is helpful in assessing predictability in terms of randomness.

The forecasting of various physical quantities is a classical problem in time-series analysis in the field of nonlinear physics, but the conceptual importance of short-term prediction in itself is not limited to cases in which the control of complex flow fields is desired. On the other hand, the applicability of the prediction method in the framework of dynamical systems theory still remains controversial, particularly when the system is governed by high dimensionality. Wall turbulence is a typical class of high-dimensional systems emerging with a rich variety of spatiotemporal dynamics with coexisting low- and high-dimensional chaotic states. Although this paper is restricted to a low-Reynolds-number condition, the OIFM has potential applications to predict the complex dynamic behavior of streamwise velocity in wall turbulence. Finally, we should consider the following point related to dynamical systems producing deterministic chaos. Various dynamical systems [50–54] that can be described by nonlinear ordinary differential equations, which were derived for wall turbulence, can produce a wide spectrum of dynamics from limit-cycle oscillations to intermittency and deterministic chaos. Such dynamical systems are simplified and one should keep in
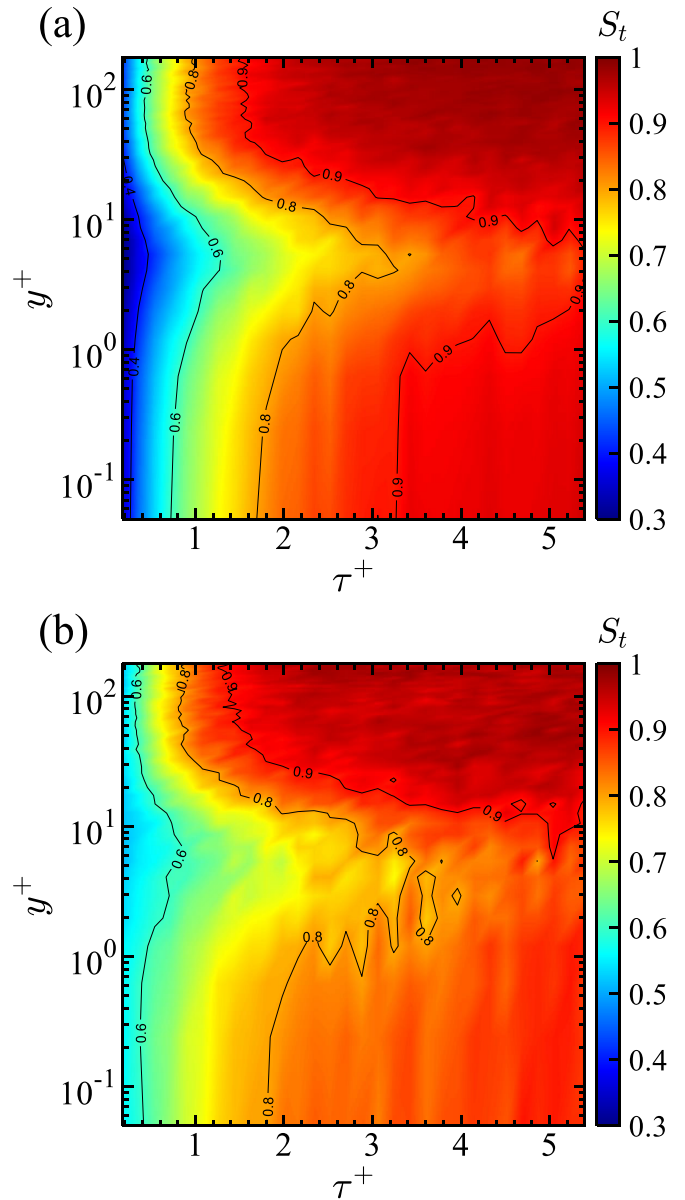
mind that the formation of a chaotic state is rather limited in actual turbulent systems. However, despite their simplicity, we need to clarify the forecastability of deterministic chaos produced by dynamical systems to obtain deeper insight into the inherent forecastability of streamwise velocity obtained by the OIFM. Comparison of the forecastability of streamwise velocity obtained by DNS with that of deterministic chaos is required in our future work.

IV. SUMMARY

We have studied the dynamic state and predictability of streamwise velocity in a low-Reynolds-number turbulent channel flow obtained by DNS from the viewpoints of symbolic dynamics and nonlinear forecasting. A low-dimensional chaotic state of streamwise velocity fluctuations emerges at a viscous sublayer, whereas it changes to a high-dimensional

chaotic state at the logarithmic layer. The possible presence of these chaotic states is clearly identified by the OPTN entropy in combination with the surrogate data method and OIFM. The predicable time of the low-dimensional chaotic state in streamwise velocity at the viscous sublayer is approximately 100 times the time resolution of DNS. The OIFM has potential for use in predicting the chaotic streamwise velocity at all the layers from the viscous sublayer to the logarithmic layer under a low-Reynolds-number channel flow.

ACKNOWLEDGMENTS

[1] E. N. Lorenz, J. Atmos. Sci. **20**, 130 (1963).

[2] H. Kantz and T. Schreiber, *Nonlinear Time Series Analysis*, 2nd ed. (Cambridge University Press, Cambridge, 2003).

[3] J. C. Sprott, *Chaos and Time-Series Analysis* (Oxford University Press, 2001).

[4] M. Small, *Applied Nonlinear Time Series Analysis: Applications in Physics, Physiology and Finance* (World Scientific, Singapore, 2005), Vol. 52.

[5] G. Sugihara and R. May, Nature (London) **344**, 734 (1990).

[6] H. Gotoda, Y. Okuno, K. Hayashi, and S. Tachibana, Phys. Rev. E **92**, 052906 (2015).

[7] H. Gotoda, M. Pradas, and S. Kalliadasis, Phys. Rev. Fluids **2**, 124401 (2017).

[8] W. Kobayashi, H. Gotoda, S. Kandani, Y. Ohmichi, and S. Matsuyama, Chaos **29**, 123110 (2019).

[9] Y. Nomi, H. Gotoda, S. Kandani, and C. Almarcha, Phys. Rev. E **103**, 022218 (2021).

[10] J. M. Amigó, *Permutation Complexity in Dynamical Systems* (Springer, Berlin, 2010).

[11] C. Bandt and B. Pompe, Phys. Rev. Lett. **88**, 174102 (2002).

[12] Q. Li and Z. Fu, Phys. Rev. E **89**, 012905 (2014).

[13] M. R. Brown, D. A. Schaffner, and P. J. Weck, Phys. Plasmas **22**, 055601 (2015).

[14] D. A. Schaffner, M. R. Brown, and A. B. Rock, Phys. Plasmas **23**, 055709 (2016).

[15] F. Olivares, L. Zunino, D. Gulich, D. G. Pérez, and O. A. Rosso, Phys. Rev. E **96**, 042207 (2017).

[16] M. Small, in *Proceedings of the 2013 IEEE International Symposium on Circuits and Systems (ISCAS2013)* (IEEE, New York, 2013).

[17] M. McCullough, M. Small, T. Stemler, and I. H. Ching, Chaos **25**, 053101 (2015).

[18] C. Aoki, H. Gotoda, S. Yoshida, and S. Tachibana, J. Appl. Phys. **127**, 224903 (2020).

[19] Y. Nomi, H. Gotoda, S. Fukuda, and C. Almarcha, Chaos **31**, 123133 (2021).

[20] J. M. Hamilton, J. Kim, and F. Waleffe, J. Fluid Mech. **287**, 317 (1995).

[21] J. Kim, P. Moin, and R. Moser, J. Fluid Mech. **177**, 133 (1987).

[22] R. D. Moser, J. Kim, and N. N. Mansour, Phys. Fluids **11**, 943 (1999).

[23] S. Hoyas and J. Jimenez, Phys. Fluids **18**, 011702 (2006).

[24] M. Lee and R. D. Moser, J. Fluid Mech. **774**, 395 (2015).

[25] Y. Yamamoto and Y. Tsuji, Phys. Rev. Fluids **3**, 012602(R) (2018).

[26] S. Hoyas, M. Oberlack, F. Alcántara-Ávila, S. V. Kraheberger, and J. Laux, Phys. Rev. Fluids **7**, 014602 (2022).

[27] S. Hochreiter and J. Schmidhuber, Neural Comput. **9**, 1735 (1997).

[28] H. Jaeger, German National Research Center for Information Technology, GMD Technical Report **148**, 13 (2001).

[29] H. Jaeger and H. Haas, Science **304**, 78 (2004).

[30] J. Pathak, Z. Lu, B. R. Hunt, M. Girvan, and E. Ott, Chaos **27**, 121102 (2017).

[31] J. Pathak, B. R. Hunt, M. Girvan, Z. Lu, and E. Ott, Phys. Rev. Lett. **120**, 024102 (2018).

[32] Z. Lu, B. R. Hunt, and E. Ott, Chaos **28**, 061104 (2018).

[33] J. Jiang and Y.-C. Lai, Phys. Rev. Res. **1**, 033056 (2019).

[34] H. Fan, J. Jiang, C. Zhang, X. Wang, and Y.-C. Lai, Phys. Rev. Res. **2**, 012080 (2020).

[35] X. Chen, T. Weng, H. Yang, C. Gu, J. Zhang, and M. Small, Phys. Rev. E **102**, 033314 (2020).

[36] T. Tokami, T. Hachijo, T. Miyano, and H. Gotoda, Phys. Rev. E **101**, 042214 (2020).

[37] M. Inubushi and S. Goto, Phys. Rev. E **102**, 043301 (2020).

[38] S. Pandey and J. Schumacher, Phys. Rev. Fluids **5**, 113506 (2020).

[39] T. Tokami, M. Toyoda, T. Miyano, I. T. Tokuda, and H. Gotoda, Phys. Rev. E **104**, 024218 (2021).

[40] V. Valori, R. Krauter, and J. Schumacher, Phys. Rev. Res. **4**, 023180 (2022).

[41] A. Asch, E. J. Brady, H. Gallardo, J. Hood, B. Chu, and M. Farazmand, Chaos **32**, 043112 (2022).

[42] K. Fukagata, N. Kasagi, and P. Koumoutsakos, Phys. Fluids **18**, 051703 (2006).

[43] J. M. Amigó, S. Zambrano, and M. A. F. Sanjuan, Europhys. Lett. **79**, 50001 (2007).

[44] C. W. Kulp and L. Zunino, Chaos **24**, 033116 (2014).

[45] T. Schreiber and A. Schmitz, Phys. Rev. Lett. **77**, 635 (1996).

[46] M. B. Kennel, R. Brown, and H. D. I. Abarbanel, Phys. Rev. A **45**, 3403 (1992).

[47] O. A. Rosso, H. A. Larrondo, M. T. Martin, A. Plastino, and M. A. Fuentes, Phys. Rev. Lett. **99**, 154102 (2007).

[48] A. N. Tikhonov, V. I. Arsenin, and F. John, *Solutions of Ill-Posed Problems*, Vol. 14 (Winston, Washington, DC, 1977).

[49] F. Takens, *Dynamical Systems and Turbulence, Warwick 1980*, edited by D. Rand and L.-S. Young, Lecture Notes in Mathematics Vol. 898 (Springer, Berlin, 1981).

[50] N. Aubry, P. Holmes, J. L. Lumley, and E. Stone, J. Fluid Mech. **192**, 115 (1988).

[51] S. Sanghi and N. Aubry, J. Fluid Mech. **247**, 455 (1993).

[52] G. Berkooz, P. Holmes, and J. L. Lumley, *Turbulence, Coherent Structures, Dynamical Systems, and Symmetry, Cambridge Monographs on Mechanics* (Cambridge University Press, Cambridge, UK, 1996).

[53] J. Moehlis, H. Faisst, and B. Eckhardt, New J. Phys. **6**, 56 (2004).

[54] A. V. G. Cavalieri, Phys. Rev. Fluids **6**, 034610 (2021).